

# We are IntechOpen, the world's leading publisher of Open Access books Built by scientists, for scientists

6,900

Open access books available

186,000

International authors and editors

200M

Downloads

Our authors are among the

154

Countries delivered to

TOP 1%

most cited scientists

12.2%

Contributors from top 500 universities



WEB OF SCIENCE™

Selection of our books indexed in the Book Citation Index  
in Web of Science™ Core Collection (BKCI)

Interested in publishing with us?  
Contact [book.department@intechopen.com](mailto:book.department@intechopen.com)

Numbers displayed above are based on latest data collected.  
For more information visit [www.intechopen.com](http://www.intechopen.com)



# Understanding the Effects of Fires on Surface Evapotranspiration Patterns Using Satellite Remote Sensing in Combination with an Energy Balance Model

Juan M. Sánchez<sup>1</sup>, Vicente Caselles<sup>2</sup> and Eva Rubio<sup>1</sup>

<sup>1</sup>University of Castilla-La Mancha

<sup>2</sup>University of Valencia  
Spain

## 1. Introduction

Forest fires are highly destructive for nature, affecting the landscape, the natural cycle of the vegetation, and the structure and functioning of ecosystems. Beyond that, they also provoke changes in the local and regional meteorology, and particularly in the surface energy flux patterns. In a fire-affected area, changes in the ecosystem structure and species composition modify the evapotranspiration ( $LE$ ) and the rest of the terms involved in the energy balance equation. Besides, these changes in the local energy balance may persist for decades (Randerson et al., 2006). There is an increasing concern among the scientific community about the effect of forest fires on climate change at this point (Randerson et al. 2006). In this work we focus on the study of the changes in the energy flux patterns after a forest fire, with particular emphasis on the evapotranspiration, which effect on the global system should be further analyzed by the radiative forcing models.

The physical characterization of the hydrological processes plays a very important role in the framework of the activities for the management of hydrological resources. Particularly, the soil-vegetation-atmosphere energy exchanges are the basis of an appropriate hydrological balance, and thus, of an appropriate planning of the hydrological resources. The fusion of physical models for estimating the hydrological balance, and particularly the evapotranspiration, with technological advances for the characterization of hydrological, hydro-geological, and atmospheric issues, is of great utility. Although there are several surface-based methods that can accurately measure surface heat fluxes at point locations, it is not feasible to use a network of these systems to create spatially distributed flux maps because of the high variability of real landscapes. As stated by Scott et al. (2000), micrometeorological approaches can only realistically provide measurements representative of a particular type of vegetation cover when there is a reasonably extensive, uniform area of that vegetation immediately upwind of the instruments. The use of remote sensing techniques supplies the frequent lack of ground-measured variables and parameters required to apply the local models at a regional scale. Modelling evapotranspiration is very sensitive to the surface features and conditions. For this reason, a regional model must

account for the surface variability. In this context, satellite remote sensing has become a basic tool since it allows us the regular monitoring of extensive areas. Different surface variables and parameters can be extracted from the combination of the multi-spectral information contained in a satellite image. The surface can be characterized with a detail depending on the spatial resolution of the sensor used. One of the goals of remote sensing is to provide us with data on barely accessible areas. This includes some regions such as, for example, forest areas where evapotranspiration retrieval is more difficult due to evident limitations on experiments.

The basis of the remote sensing models using thermal infrared data for determining evapotranspiration is the direct relationship between surface thermodynamic temperature and energy balance, which has long been recognized by meteorologists and hydrologists. The surface thermodynamic temperature can be obtained from the brightness temperature after atmospheric and emissivity corrections. Monteith (1973) proposed a single source model based on a convection analogue to Ohm's Law to obtain the sensible heat flux. However, the evaluation of this single source model showed important limitations for partial canopy cover conditions (Hall et al. 1992). Two-source (soil + vegetation) layer models have been developed to accommodate partial canopy cover conditions considering energy exchange between soil and canopy components (Shuttleworth & Wallace, 1985; Choudhury & Monteith, 1988, Norman et al., 1995, Sánchez et al., 2008).

Inoue and Moran (1997) proposed a simple method to estimate daily values of actual canopy transpiration. The method utilizes instantaneous differences of canopy and air temperature around mid-day as a major input. Results were found to be well correlated to those measured by sap-flow heat balance method in soybean canopies. Anderson et al. (1997) presented an operational two-source (soil+vegetation) model for evaluating the surface energy balance given measurements of the time rate of change in radiometric surface temperature during morning hours. Using this model, the need for ancillary measurements of near-surface air temperature is eliminated. The performance of this model was evaluated in comparison with data collected during the first International Satellite Land Surface Climatology Project field experiment, in Kansas, and the Monsoon '90 experiment, conducted in southern Arizona. Comparisons yielded uncertainties comparable to measurement errors typical of standard micrometeorological methods for flux estimation. Chehbouni et al. (2001) used dual angle observations of radiative surface temperature in conjunction with a two-layer model to derive sensible heat flux over the Semi Arid Land Surface Atmosphere program (SALSA) in Mexico. The average error was about 23%. Moran et al. (1994) introduced a water deficit index for evaluating evapotranspiration rates of both full cover and partially vegetated sites. This index can be computed using remotely sensed measurements of surface temperature and reflectance with limited on-site meteorological data. Comparison with simulations of a two-source energy balance model showed accurate estimates of field evapotranspiration rates. French et al. (2005) used data from ASTER collected over an experimental site in central Iowa, in the framework of the Soil moisture Atmosphere Coupling Experiment (SMACEX), to retrieve surface energy fluxes. Two different approaches, designed to account for the spatial variability, were considered: the Two-Source Energy Balance model (TSEB) and the Surface Energy Balance Algorithm for Land model (SEBAL). Comparison of the results with eddy covariance measurements showed better agreement using the TSEB model with average deviations lower than 20 W m<sup>-2</sup>. These results were also supported by Li et al. (2005). These authors compared local model output using two different versions of the TSEB (series and parallel) with tower-

based flux observations. Root mean square differences ranged from 20 to 50 W m<sup>-2</sup>. In this case, land surface temperatures were derived from high resolution Landsat Thematic Mapper (TM) and Enhanced Thematic Mapper (ETM+) scenes and aircraft imagery. Su et al. (2005) also used SMACEX data to evaluate the Surface Energy Balance System (SEBS) model using both high-quality local-scale data and high-resolution remote sensing data from the Landsat ETM+.

Despite the wide variety of remote sensing-based works and proposed models on evapotranspiration retrieval, there is not a generalized agreement about the most appropriate model depending on the application area. In this work, we present a methodology focused on the *LE* retrieval from high-resolution satellite data. The bases of this method are the energy balance equation and a Simplified Two-Source Energy Balance (STSEB) model proposed by Sánchez et al. (2008) for estimating instantaneous surface fluxes. This model was validated over a variety of surface conditions with good results. Also, an exhaustive analysis of sensitivity to typical uncertainties (assumed for a regional variability) in the required inputs was performed by these authors (Sánchez et al., 2008, 2009). The combination of the STSEB model with remote sensing techniques results in an operational methodology to retrieve evapotranspiration at a regional scale from remote sensing and local meteorological data. In this work we show the application of this methodology to Landsat imagery and a particular region in Spain, but it could be extended to other high-resolution sensors, and what it is even more interesting, to any other regions in the world.

In this work we focus on an area, located in Almodovar del Pinar, Cuenca (Spain), affected by a forest fire in the summer of 2001. This fire destroyed 172 ha of pine forest and shrubland. After the fire this area became an intensive study site. Our objective is to quantify the effect of this forest fire in terms of net radiation, soil and sensible heat fluxes, and evapotranspiration in the two land cover classes dominant in the area, mature pine forests and shrublands. With this aim we applied the STSEB model (Sánchez et al., 2008) to a set of 5 images Landsat 5 Thematic-Mapper (TM) corresponding to the period July 2007-July 2008.

## 2. Methodology

The governing equation is the Energy Balance Equation (EBE) of the land surface, which models a system formed by vegetation, surrounding soil, and atmosphere:

$$R_n = G + H + LE \quad (1)$$

where  $R_n$  is the net radiation flux (W m<sup>-2</sup>),  $G$  is the soil heat flux (W m<sup>-2</sup>),  $H$  is the sensible heat flux (W m<sup>-2</sup>) and  $LE$  is the latent heat flux in the atmosphere boundary layer (W m<sup>-2</sup>). According to Seguin and Itier (1983):

$$\frac{H_d}{R_{nd}} = \frac{H_i}{R_{ni}} \quad (2)$$

where the subscripts  $i$  and  $d$  refer to instantaneous and daily fluxes, respectively.

On diurnal timescales,  $G$  can constitute an important contribution to the EBE (Choudhury, 1987; Santanello and Friedl, 2003). However, at a daily scale  $G$  can be neglected in equation (1) (Seguin and Itier, 1983; Lagouarde and McAneney, 1992; Sánchez et al., 2007), and  $LE$  can be obtained from equations (1) and (2) as:

$$LE_d = \frac{R_{nd}}{R_{ni}}(R_{ni} - H_i) \quad (3)$$

Using equation (3),  $LE_d$  can be obtained from the instantaneous values of  $R_n$  and  $H$  at a particular time of day, and the relative net radiation contribution at that time when global radiative exchange is integrated,  $R_{nd}/R_{ni}$ .

The instantaneous net radiation is estimated by establishing a balance between the long-wave and the short-wave radiation:

$$R_n = (1 - \alpha)S + \varepsilon L_{sky} - \varepsilon \sigma T_R^4 \quad (4)$$

where  $S$  is the solar global radiation ( $\text{W m}^{-2}$ ),  $T_R$  is the radiometric land surface temperature,  $\alpha$  is the surface albedo,  $\varepsilon$  is the surface effective emissivity, and  $\sigma$  is the Stefan-Boltzmann constant.  $L_{sky}$  is the incident long-wave radiation ( $\text{W m}^{-2}$ ).

In the STSEB approach proposed by Sánchez et al. (2008), the ground surface is divided in two components, canopy and soil surrounding (Fig. 1). According to this configuration, the total sensible heat flux is obtained by the addition between the soil and canopy contributions,  $H_s$  and  $H_c$ , respectively:

$$H = P_v H_c + (1 - P_v) H_s \quad (5)$$

In this equation,  $P_v$  is the vegetation cover, and  $H_s$  and  $H_c$  are expressed as:

$$H_c = \rho C_p \frac{T_c - T_a}{r_a^h} \quad (6a)$$

$$H_s = \rho C_p \frac{T_s - T_a}{r_a^a + r_a^s} \quad (6b)$$

where  $\rho C_p$  is the volumetric heat capacity of air ( $\text{J K}^{-1}\text{m}^{-3}$ ),  $T_a$  is the air temperature at a reference height (K),  $T_c$  and  $T_s$  are the canopy and soil radiometric temperatures, respectively,  $r_a^h$  is the aerodynamic resistance to heat transfer between the canopy and the reference height ( $\text{m s}^{-1}$ ),  $r_a^a$  is the aerodynamic resistance to heat transfer between the point  $z_0+d$  ( $z_0$ : roughness length,  $d$ : displacement height) and the reference height ( $\text{m s}^{-1}$ ),  $r_a^s$  is the aerodynamic resistance to heat flow in the boundary layer immediately above the soil surface ( $\text{m s}^{-1}$ ). A summary of the expressions to estimate these resistances using the wind speed and crop height, and more details about the STSEB model can be seen in Sánchez et al. (2008).

Finally, the instantaneous soil heat flux can be obtained as a fraction of the net radiation:

$$G = C_G(1 - P_v)R_n \quad (7)$$

In this work we used a value of  $C_G=0.275$  (mean value of the usual range 0.15-0.40).

## 2.1 Surface temperature and emissivity

Landsat-TM and ETM+ sensors possess a unique thermal band with a spectral range of 10.4-12.5  $\mu\text{m}$ , and an effective wavelength of 11.457  $\mu\text{m}$ . This limitation does not allow to apply split-window methods neither Temperature/Emissivity Separation (TES) methods.

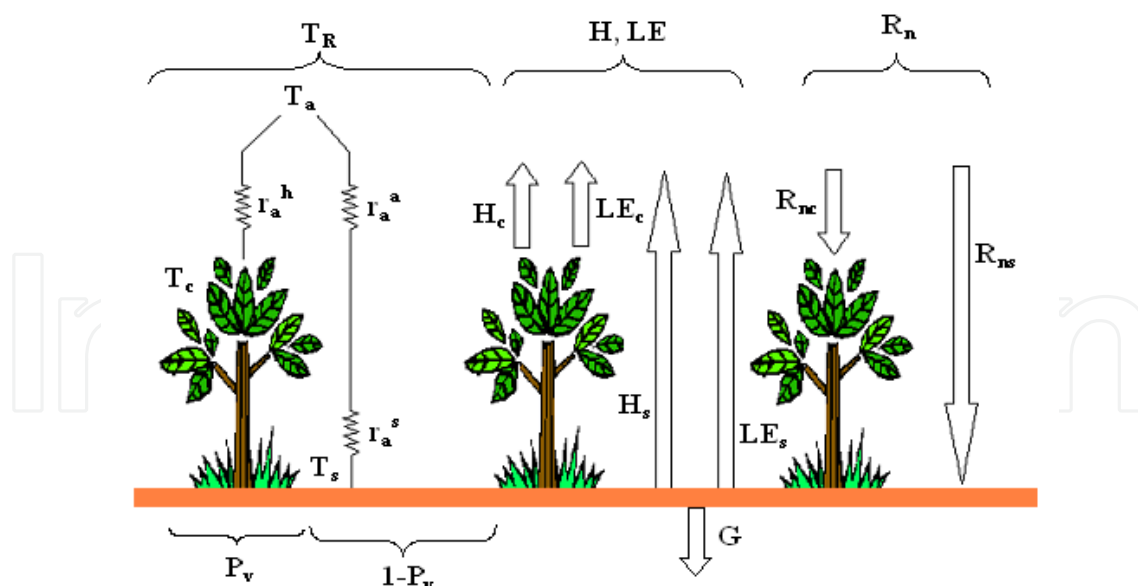


Fig. 1. Scheme of resistances and flux partitioning between soil and canopy, corresponding to the STSEB approach. Symbols are defined in the text.

Therefore, a single-channel method, based on the radiative transfer equation, was used. The remotely measured channel radiance,  $R_i$ , consist of two main contributions: (1) the radiance at surface level, which is attenuated by the absorption of the atmosphere between the surface and the instrument, characterized by the atmospheric transmittance,  $\tau_i$ , and (2) the upwelling sky radiance emitted by the atmosphere in the viewing direction,  $L_{i \text{ atm}}^{\uparrow}(\theta)$ , so that  $R_i$ , in agreement with the radiative transfer equation, is stated as:

$$R_i = \left[ \varepsilon_i B_i(T_R) + [1 - \varepsilon_i] L_{i \text{ atm hem}}^{\downarrow} \right] \tau_i + L_{i \text{ atm}}^{\uparrow} \quad (8)$$

where  $B_i(T_R)$  is Planck's function for a temperature  $T_R$ ,  $\varepsilon_i$  is the surface emissivity and  $L_{i \text{ atm hem}}^{\downarrow}$  is the hemispheric downwelling sky irradiance divided by  $\pi$  (Lambertian reflection assumed). Radiosounding data were introduced into the MODTRAN 4.0 code (Berk et al., 1999) to get estimates of  $\tau_i$ ,  $L_{i \text{ atm}}^{\uparrow}(\theta)$  and  $L_{i \text{ atm hem}}^{\downarrow}$ . Although equation (8) depends on the observation angle ( $\theta$ ), the nadir view provides good results for Landsat-TM and ETM+. A simple and operational equation proposed by Valor & Caselles (2005) was used to estimate the surface emissivity from the knowledge of the vegetation cover,  $P_v$ , and the emissivities of the soil and canopy components,  $\varepsilon_s$  and  $\varepsilon_c$ , respectively.

$$\varepsilon = \varepsilon_c P_v + \varepsilon_s (1 - P_v) (1 - 1.74 P_v) + 1.7372 P_v (1 - P_v) \quad (9)$$

Equation (9) includes the effect of the geometrical distribution of the vegetated surface and also the internal reflections. Typical emissivity values can be assumed for  $\varepsilon_c$  and  $\varepsilon_s$  (Rubio et al., 1997, 2003).

## 2.2 Vegetation cover

Bands 3 (0.63-0.69  $\mu\text{m}$ ) and 4 (0.76-0.90  $\mu\text{m}$ ) of TM and ETM+ were used to estimate NDVI. Previously, visible and near-infrared bands were corrected of atmospheric effects using the radiosounding data and the MODTRAN 4.0 code. For this purpose, the at-surface channel reflectivity,  $\rho_i$ , is calculated with the following equation:



$$\rho_i = \frac{\pi(R_i - L_{i\ atm}^{\uparrow})d^2}{\tau_i(ESUN_i \cos(\alpha)\tau(\alpha) + L_{i\ atm\ hem}^{\downarrow})} \quad (10)$$

where  $\tau(a)$  is the atmospheric transmissivity between the sun and the surface,  $a$  is the zenithal solar angle,  $ESUN_i$  is the spectral solar irradiance on the top of the atmosphere, and  $d$  is the Earth-Sun distance.

Vegetation cover was obtained through the expression (Valor & Caselles, 1996):

$$P_v = \frac{\left(1 - \frac{NDVI}{NDVI_s}\right)}{\left(1 - \frac{NDVI}{NDVI_s}\right) - K\left(1 - \frac{NDVI}{NDVI_v}\right)} \quad (11)$$

where the coefficient  $K$  is obtained by:

$$K = \frac{R_{NIR_v} - R_{RED_v}}{R_{NIR_s} - R_{RED_s}} \quad (12)$$

where  $R_{NIR}$  is the near infrared reflectivity, and  $R_{RED}$  is the red visible reflectivity. The subscript  $v$  and  $s$  correspond to completely vegetated and unvegetated areas, respectively, selected by looking at the spectral contrast among bands 3-5. These selected areas were also used to estimate  $T_c$  and  $T_s$ , required in equations (6a) and (6b), respectively, from the land surface temperature maps generated.

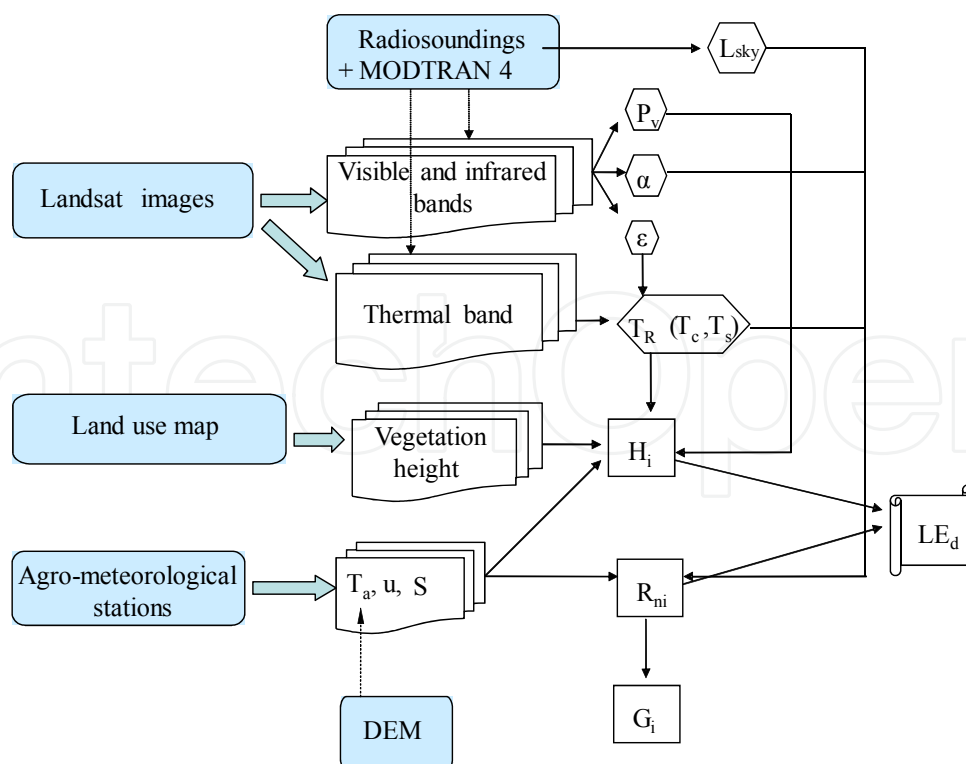


Fig. 2. Scheme of the methodology proposed to retrieve actual daily evapotranspiration at a regional scale.

### 2.3 Albedo

Some authors such as Dubayah (1992), Duguay (1992), etc, divided the spectral region from 0.3 to 3.0  $\mu\text{m}$  into 10 spectral bands to estimate surface albedo. Each band has a different integrating weight according to the typical vegetation spectral reflectance pattern. In this paper, the surface albedo is integrated by using the equation (Dubayah, 1992):

$$\alpha = 0.221\rho_1 + 0.162\rho_2 + 0.102\rho_3 + 0.354\rho_4 + 0.059\rho_5 + 0.0195\rho_7 \quad (13)$$

where  $\rho_i$  is the corrected reflectivity for the  $i$  band of TM or ETM+. The average error of the calculated surface net radiation, using equation (12) for estimating the albedo, is around 2% when comparing to field measurements (Dubayah, 1992).

### 2.4 Meteorological variables

Ancillary meteorological data are required to complete the set of variables and parameters involved in the previously shown scheme of equations. Air temperature,  $T_a$ , is necessary in equations (6a) and (6b) to estimate the exchange of sensible heat flux between the surface and the atmospheric boundary layer. Wind speed,  $u$  ( $\text{m s}^{-1}$ ), is required in the expressions to calculate the aerodynamic and soil resistances taking part in the STSEB model (Sánchez et al., 2008). The global solar radiation,  $S$ , and the incident long-wave radiation,  $L_{sky}$ , are necessary in the net radiation balance (Eq. 4). All these variables, except  $L_{sky}$ , are continuously registered in typical agro-meteorological stations, regional maps can be created by interpolating the data registered in a network of stations distributed within the study area. Regarding  $L_{sky}$ , due to its known spatial homogeneity across a relative extensive area (Humes et al., 2002), a single value of this variable can be used for each image, and it can be obtained from launched radiosoundings. Sánchez et al. (2008) showed that particular care must be taken with the air temperature when the STSEB model is applied since an uncertainty in  $T_a$  can lead to a significant error in the evapotranspiration retrieval. For this reason a Digital Elevation Model (DEM) can be considered in order to obtain more reliable maps of this meteorological variable.

A scheme of the methodology exposed is shown in Figure 2.



Fig. 3. (a) Location of the study site. (b) Overview of the burned area, and the Bowen station placed in site. (c) Overview of the forested\_c areas, and the meteorological tower placed in site.

### 3. Study site

The study site is a forest area, with some inserted crop fields, located in Almodóvar del Pinar, Cuenca ( $39^{\circ} 40' \text{N}$ ,  $1^{\circ} 50' \text{W}$ , 950 m above sea level) (Fig. 3a). Climate is mediterranean,



with warm and dry summers, and cool winters. The dominant tree species is *Pinus pinaster* Ait., but many other species coexist. In the summer of 2001, a fire affected a total of 172 ha of which 113 ha were covered by pines and 59 ha by shrubs (Fig. 4). After the fire, the species *Quercus ilex* L. was occupying the burned area as a consequence of a natural regeneration process. Four 125×125 m test sites, two inside and two outside the burned area perimeter, were selected for this study, as samples of both pine areas and shrublands. Test sites outside the fire perimeter were called control sites (\_c). Environmental conditions in these control sites mimic those in the two test sites inside the burned perimeter in case the fire had never happened. A meteorological tower was placed in the *Forest\_c* area (Fig. 3c) with the instrumentation necessary to measure air temperature and wind speed, at several heights, as well as incident solar radiation, precipitation, etc. Also, a Bowen station was set up in the *Forest* site in september 2007 (Fig. 3b). Moreover, we selected a nearby area representative of a mature holm oak forest to analyze the effect of the fire on a future scenario in which pines are replaced by holm oaks as the dominant species. For this work we have used a set of 5 Landsat 5-TM scenes (19 July 2007, 4 August 2007, 28 September 2007, 2 May 2008, 21 July 2008) with a spatial resolution of 30 m for the visible and near infrared bands, and 120 m for the thermal band (all bands were rescaled to 25 m). Also, the atmospheric profiles required for the atmospheric correction of the images were obtained from the website <http://atm-corr.gsfc.nasa.gov/>.

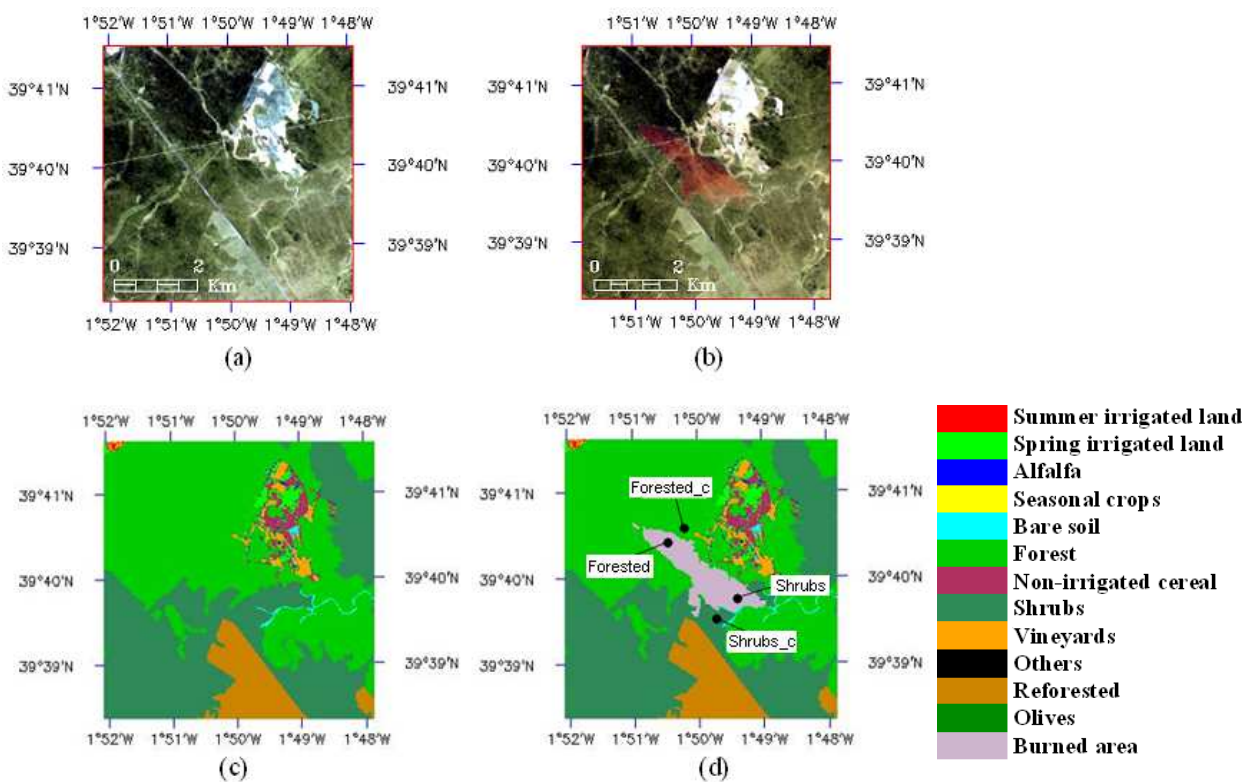


Fig. 4. Study site: (a) False color composition (7,5,3) from a L7-ETM+ image for the 8 June 2001 (prior fire), (b) Idem for the 26 July 2001 (post- fire), (c) Land use map before the fire, (d) Idem after the fire.

4. Results

4.1 Comparison with control areas

Firstly, the similarity between the control sites and the fire-affected areas was tested. For this, two Landst 7-ETM+ were used, before and after the fire date (8 June 2001 and 26 July 2001). Using digital count data, without further processing, we compared values obtained in both sites for each one of the 7 Landsat channels. Figure 5a shows this comparison prior the fire. Differences between the control areas and those affected by the fire a few days afterwards are negligible. However, these differences are evident after the fire (Fig. 5b). A significant increase is observed in values of bands 6 (thermal infrared) and 7, whereas values decrease in band 4 (near infrared), consequence of the vegetation disappearance.

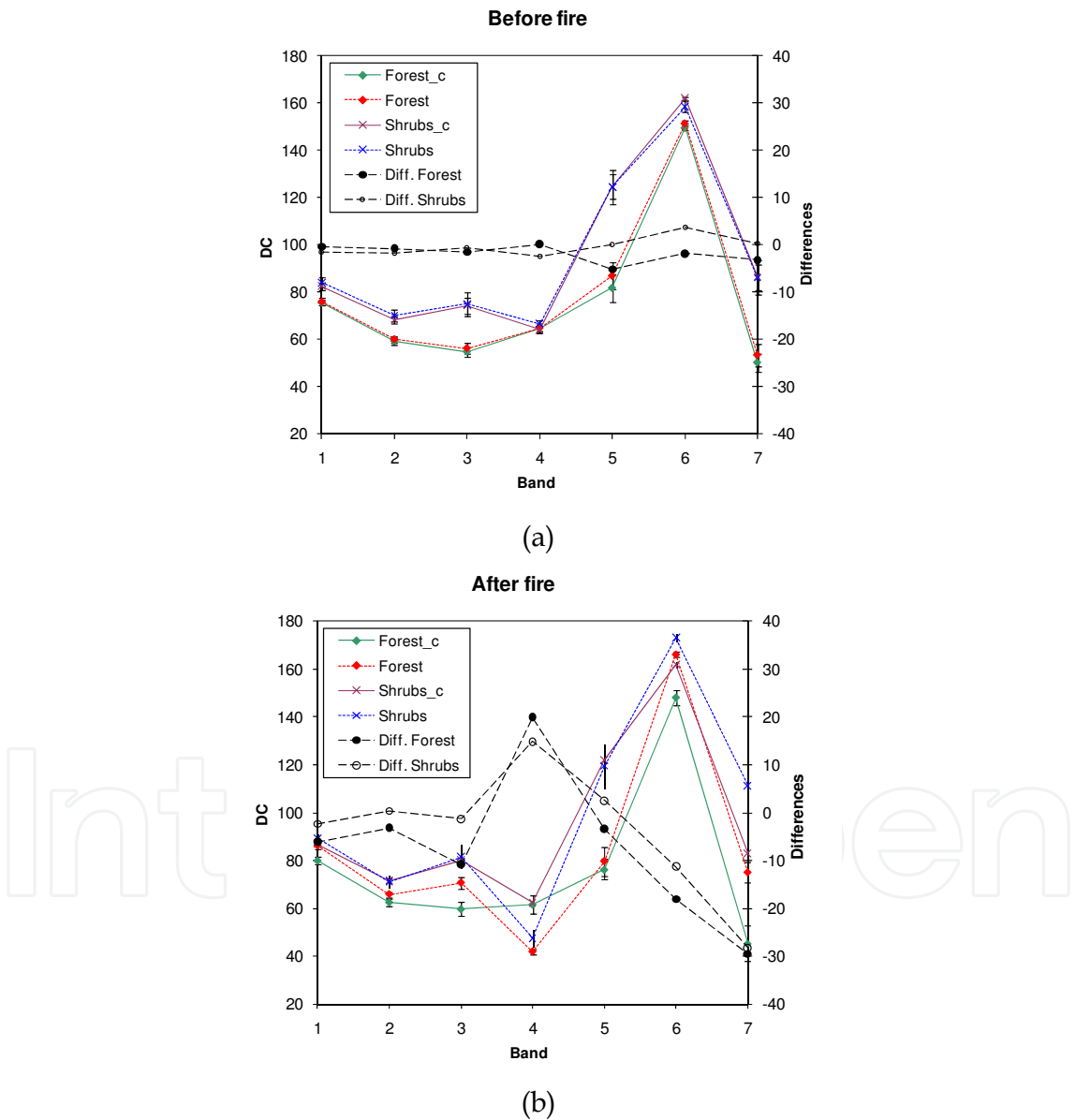


Fig. 5. Average digital count values, and their corresponding error bars, for each one of the selected areas, and differences with their corresponding control areas, (a) before the fire, (b) after the fire. Spectral ranges for the different bands: (1) 0.45-0.52  $\mu\text{m}$ , (2) 0.52-0.60  $\mu\text{m}$ , (3) 0.63-0.69  $\mu\text{m}$ , (4) 0.76-0.9  $\mu\text{m}$ , (5) 1.55-1.75  $\mu\text{m}$ , (6) 10.4-12.5  $\mu\text{m}$ , (7) 2.08-2.35  $\mu\text{m}$ .

4.2 Comparison with observed fluxes

Once processed with MODTRAN the atmospheric profiles for each one of the Landsat images, we obtained the atmospheric parameters required for the atmospheric correction of the different bands. Inputs required in equations (6), (11), and (12), were extracted after selecting a full covered area and a bare soil area. Merging the satellite information with values of air temperature, wind speed and global radiation, the data set we need is completed. Figure 6 shows, as an example, maps generated from the 28 September 2007 image. Three of the five scenes in the present study are concurrent with ground flux measurements, which allows us to compare flux results with values registered in the Bowen station located in the *forest* site. Table 1 lists the values estimated and those ground-measured. A good agreement is shown between predicted and observed fluxes. To sum up, relative errors of 7% ( $40\text{ W m}^{-2}$ ), 12% ( $10\text{ W m}^{-2}$ ), 19% ( $70\text{ W m}^{-2}$ ), and 21% ( $21\text{ W m}^{-2}$ ) are obtained for  $R_n$ ,  $G$ ,  $H$ , and  $LE$ , respectively, at a instantaneous scale, while at a daily scale errors are 6% ( $11\text{ W m}^{-2}$ ), 3% ( $4\text{ W m}^{-2}$ ), and 22% ( $10\text{ W m}^{-2}$ ) for  $R_n$ ,  $H$ , and  $LE$ , respectively. Note that this is not a robust validation, however the model has been previously tested under different coverages (Sánchez et al., 2008, 2009).

Date	Instantaneous		Daily	
	Observed / Estimated		Observed / Estimated	
<b>R<sub>n</sub></b>				
28 Sep.2007	492	544±7	118	130.6±1.7
2 May 2008	633	640±6	187	192.0±1.8
21 Jun.2008	653	626±7	203	194±2
<b>G</b>				
28 Sep.2007	123	98±6		
2 May 2008	134	125±6		
21 Jun.2008	101	105±7		
<b>H</b>				
28 Sep.2007	305	390±30	92	91±7
2 May 2008	386	365±19	118	110±6
21 Jun.2008	427	375±25	122	116±8
<b>LE</b>				
28 Sep.2007	64	60±40	25	38±8
2 May 2008	113	150±30	51	83±7
21 Jun.2008	126	150±40	61	78±9

Table 1. Estimated and observed values of the surface energy fluxes ( $\text{Wm}^{-2}$ ) at the forest site.

4.3 Analysis of the fire effect

Average values of the fluxes and most significant parameters of the model were obtained for each one of the test sites and dates. Note that the fire event occurred in 2001, and 6 years is enough time for the shrublands to recover its original stage (prior the fire); however, it is a very short time period for the forested area. This can be seen in the average values of NDVI and  $P_v$  listed in Table 2. A similar effect can be observed in terms of surface temperature. In the forest site  $T_R$  values are, in average,  $6\text{ }^{\circ}\text{C}$  higher in the burned area, whereas in the

shrubs site, temperature is 0.6 °C lower in the burned area. These differences are in agreement with those observed by other authors in similar studies (Amiro et al., 1999). After those 6 years, the effect of the fire on the energy flux pattern has almost disappeared in the shrub sites, while it is still significant in the forested sites. Figure 7 shows the plots with the average values (for the 5 study dates) of the differences in terms of energy fluxes between calculated values for the forested and shrub test sites and their respective control sites. The increase in albedo and  $T_R$  produces a decrease in both shortwave and longwave net radiation, yielding an average net decrease in  $R_{ni}$  of  $54\pm5\text{ W m}^{-2}$ . The opposite effect is observed in  $G_i$ , with an average increase of  $43\pm10\text{ W m}^{-2}$ . At a daily scale the average decrease in  $R_{nd}$  results  $15\pm3\text{ W m}^{-2}$ . Sensible heat flux is higher in the burned area, in average  $160\pm40\text{ W m}^{-2}$  at the time of the satellite overpass, and  $45\pm9\text{ W m}^{-2}$  at daily scale, whereas latent heat flux is lower,  $250\pm50\text{ W m}^{-2}$  at the time of the satellite overpass, and  $61\pm7\text{ W m}^{-2}$  ( $2.1\pm0.2\text{ mm/day}$ ) at daily scale. Therefore, even though the effect of the fire on the total net radiation is not very important, it is significant the increase in the Bowen ratio ( $H/LE$ ), and the drastic decrease in the evapotranspiration in forested areas.

Date	Forest		Shrub		Mature holm oak forest
	Control	Burned	Control	Burned	
Albedo					
19 Jul. 2007	0.117	0.140	0.124	0.139	0.144
4 Aug.2007	0.119	0.134	0.126	0.138	0.143
28 Sep.2007	0.095	0.115	0.098	0.12	0.132
2 May 2008	0.116	0.127	0.119	0.128	0.135
21 Jun.2008	0.114	0.131	0.120	0.134	0.138
NDVI					
19 Jul. 2007	0.43	0.29	0.32	0.31	0.35
4 Aug.2007	0.40	0.28	0.29	0.29	0.33
28 Sep.2007	0.63	0.38	0.42	0.38	0.45
2 May 2008	0.46	0.28	0.29	0.29	0.37
21 Jun.2008	0.44	0.33	0.35	0.35	0.39
P <sub>v</sub>					
19 Jul. 2007	0.58	0.33	0.37	0.36	0.44
4 Aug.2007	0.52	0.29	0.31	0.31	0.39
28 Sep.2007	0.74	0.34	0.41	0.35	0.46
2 May 2008	0.63	0.29	0.33	0.32	0.48
21 Jun.2008	0.61	0.39	0.43	0.44	0.51
T <sub>R</sub> (°C)					
19 Jul. 2007	36.8	42.9	42.1	41.2	39.5
4 Aug.2007	37.5	43.5	43.3	42.8	40.6
28 Sep.2007	21.4	27.1	26.0	25.8	24.5
2 May 2008	18.6	25.3	22.1	21.4	22.0
21 Jun.2008	26.2	33.1	31.6	30.7	30.0

Table 2. Average values of the main radiometric parameters for all study sites and dates.



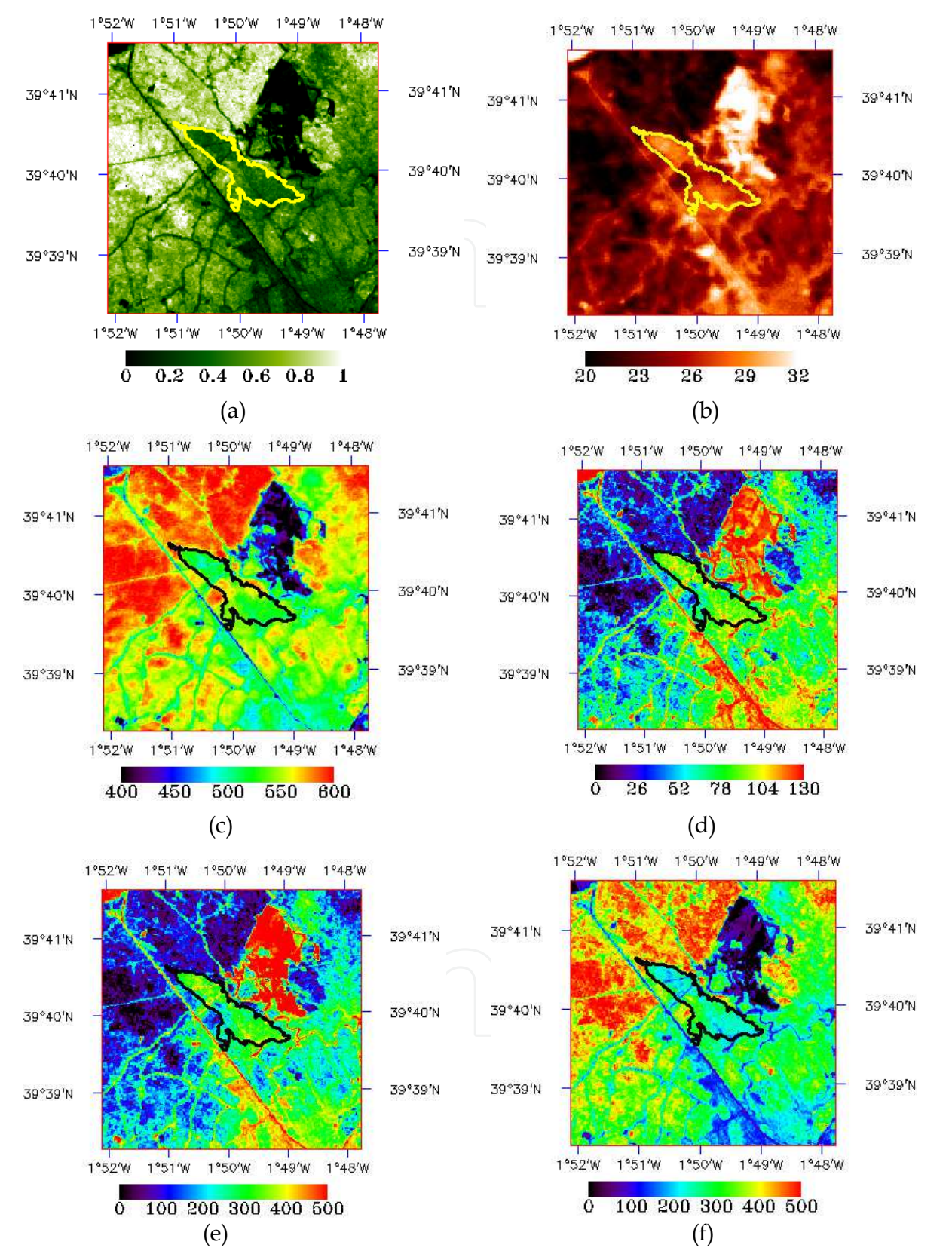


Fig. 6. Instantaneous values of: (a)  $P_v$ , (b)  $T_R$  ( $^{\circ}\text{C}$ ), (c)  $R_n$  ( $\text{W m}^{-2}$ ), (d)  $G$  ( $\text{W m}^{-2}$ ), (e)  $H$  ( $\text{W m}^{-2}$ ) and (f)  $LE$  ( $\text{W m}^{-2}$ ), obtained from the L5-TM image corresponding to the date 28 September 2007.



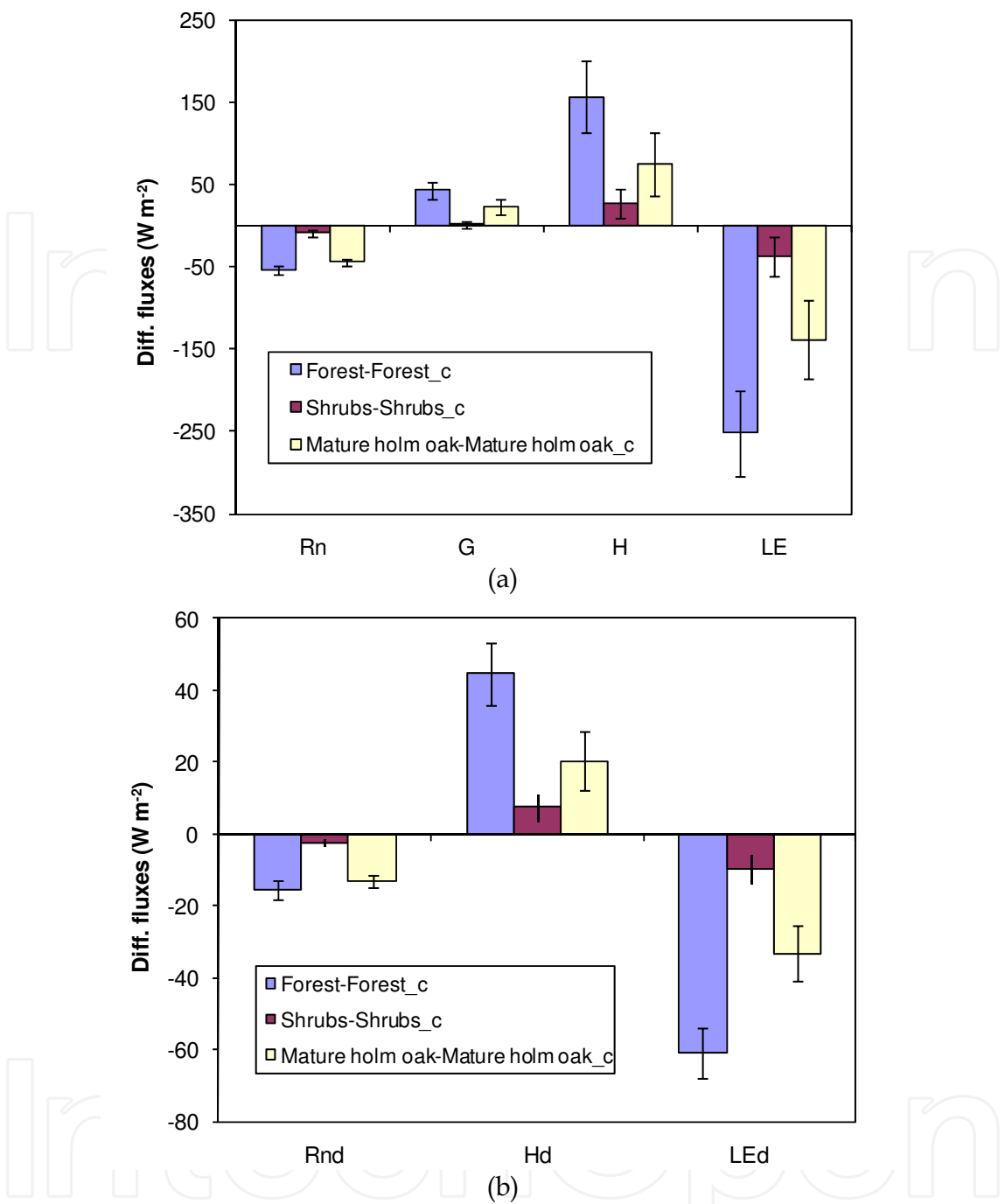


Fig. 7. Average values of the differences between burned and non-burned areas in terms of  $R_n$ ,  $G$ ,  $H$ , and  $LE$ : (a) Instantaneous fluxes; (b) Daily fluxes. Error bars represent the standard deviations of the averages.

Figure 7 shows also the effect of the fire in a future scenario in which the burned area has been naturally reforested and a mature holm oak forest is occupying the area. With this aim, differences between the forest\_c area and a selected area representative of the mature holm oak forest are shown. Note that the net radiation is barely affected by the pass of the years. However, differences in terms of  $G$ ,  $H$ , and  $LE$  would be half reduced at both instantaneous and daily scales. Despite this reduction significant differences in the flux patterns remain when replacing the pine with the holm oak as the dominant species. Thus we might

conclude a irreversible reduction above 1 mm/day in the fire-affected area, even many years after the event. It would be desirable to expand this study to coming years and perform a more detailed temporal monitoring of the flux patterns in the area.

## 5. Conclusions

We have analyzed the effect of a fire on the energy flux pattern in a mediterranean forest area affected by a fire in the summer of 2001, located in a central Spain region. High resolution satellite imagery has been used, and two different ecosystems, a pines area and a shrublands area, have been studied. Maps of the different fluxes have been obtained for each one of the 5 Landsat 5-TM images, applying the described methodology. Validation with ground measurements shows relative errors of 7, 12, 19, and 21% for  $R_n$ ,  $G$ ,  $H$ , and  $LE$ , respectively, at a instantaneous scale, and of 6, 3, and 22% for  $R_n$ ,  $H$ , and  $LE$ , respectively, at a daily scale. These results are in agreement with those obtained in recent validations of the presented methodology under different land cover types. The effect of the fire in the shrubland test site is negligible after 6 years. However, in the forested test site, an increase in  $H$  over 150 W m<sup>-2</sup>, and a decrease in  $LE$  over 250 W m<sup>-2</sup>, still remain around midday. At a daily scale the increase in  $H$  results 40 W m<sup>-2</sup>, and the decrease in  $LE$  over 60 W m<sup>-2</sup> (2.1 mm/day). This is mainly due to fire effects such as the decrease in  $P_v$  of almost 30%, or the increase in  $T_R$  of 6 °C approximately. Additional comparison with a nearby area covered by mature holm oak allows the analysis of the effect of the replacement of the pine with the holm oak as the dominant species, consequence of a natural post-fire regeneration process. The main result is the irreversible reduction of more than 1 mm/day produced in terms of daily evapotranspiration, that might have an impact on the local hydrological cycle and also on the local, or even regional, meteorology.

## 6. Acknowledgements

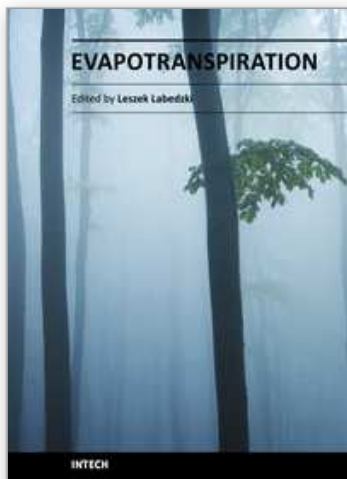
This work has been funded by the Spanish Science and Innovation Ministry (Projects CGL2007-64666/CLI, CGL2010-17577/CLI, AGL2009-13124, CSD2008-00040, CGL2008-04047, and Juan de la Cierva contract of J. M. Sánchez), Generalitat Valenciana (project PROMETEO/2009/086) and the JCCM (project ECOFLUX II, Ref: PCC08-0109).

## 7. References

- Amiro, B. D., Macpherson, J. I., & Desjardins, R. L. (1999). BOREAS flight measurements of forest-fire effects on carbon dioxide and energy fluxes. *Agricultural and Forest Meteorology*, 96, 199-208.
- Anderson, M. C., Norman, J. M., Diak, G. R., Kustas, W. P., & Mecikalski, J. R. (1997). A two-source time integrated model for estimating surface fluxes using thermal infrared remote sensing. *Remote Sensing of Environment*, 60, 195-216.
- Berk, A., Anderson, G. P., Acharya, P. K., Chetwynd, J. H., Bernstein, L. S., Shettle, E. P., Matthew, M. W., & Adler-Golden, S. M. (1999). MODTRAN 4 user's manual. In: *Air Force Research Laboratory, Space Vehicles Directorate* (Hascom AFB, MA: Air Force Materiel Command).
- Chehbouni, A., Nouvellon, Y., Lhomme, J.-P., Watts, C., Boulet, G., Kerr, Y. H., Moran, M.S., & Goodrich, D. C. (2001). Estimation of surface sensible heat flux using dual angle

- observations of radiative surface temperature. *Agricultural and Forest Meteorology*, 108, 55-65.
- Choudhury, B. J., Idso, S. B., & Reginato, R. J. (1987). Analysis of an empirical model for soil heat flux under a growing wheat crop for estimating evaporation by an infrared-temperature based energy balance equation. *Agricultural and Forest Meteorology*, 39, 283-297.
- Choudhury, B., & Monteith, J. (1988). A four-layer model for the heat budget of homogeneous land surfaces. *Quarterly Journal of the Royal Meteorological Society*, 114, 373-398.
- Dubayah, R. (1992). Estimating net solar radiation using Landsat Thematic Mapper and digital elevation data. *Water Resource Research*, 28, 2469-2484.
- Duguay, C. R. (1992). Estimating surface reflectance and albedo from Landsat-5 thematic Mapper over rugged terrain. *Photogrammetric Engineering & Remote Sensing*, 58, 551-558.
- French, A. N., Jacob, F., Anderson, M. C., Kustas, W. P., Timmermans, W., Gieske, A., Su, Z., Su, H., McCabe, M. F., Li, F., Prueger, J., & Brunsell, N. (2005). Surface energy fluxes with the Advanced Spaceborne Thermal Emission and Reflection radiometer (ASTER) at the Iowa 2002 SMACEX site (USA). *Remote Sensing of Environment*, 99 (1-2), 55-65.
- Hall, F., Huemmrich, K., Goetz, S., Sellers, P., & Nickerson, J. (1992). Satellite remote sensing of surface energy balance: Success, failures and unresolved issues in FIFE. *Journal of Geophysical Research*, 97, 19061-19089.
- Humes, K., Ardí, R., Kustas, W.P., Prueger, J., & Starks, P. (2002). High spatial resolution mapping of surface energy balance components with remotely sensed data. In: *Thermal Remote Sensing in Land Surface Processes*, New York, CRC Press. pp. 110-132.
- Inoue, Y., & Moran, M. S. (1997). A simplified method for remote sensing of daily canopy transpiration-a case study with direct measurements of canopy transpiration in soybean canopies. *International Journal of Remote Sensing*, 18 (1), 139-152.
- Lagouarde, J.-P., & McAneney, K. J. (1992). Daily sensible heat flux estimation from a single measurement of surface temperature and maximum air temperature. *Boundary-Layer Meteorology*, 59, 341-362.
- Li, F., Kustas, W. P., Prueger, J. H., Neale, C. M. U., & Jackson, T. J. (2005). Utility of Remote Sensing based two-source energy balance model under low and high vegetation cover conditions. *Journal of Hydrometeorology*, 6 (6), 878-891.
- Monteith, J. L. (1973). *Principles of environmental physics*, London, Edward Arnold Publisher, 241 pp.
- Moran, M. S., Clarke, T. R., Inoue, Y., & Vidal, A. (1994). Estimating crop water deficit using the relation between surface-air temperature and spectral vegetation index. *Remote Sensing of Environment*, 49, 246-263.
- Norman, J. M., Kustas, W., & Humes, K. (1995). A two-source approach for estimating soil and vegetation energy fluxes from observations of directional radiometric surface temperature. *Agricultural and Forest Meteorology*, 77, 263-293.
- Randerson, J. T., Liu, H., Flanner, M. G., Chambers, S. D., Jin, Y., Hess, P. G., Pfister, G., Mack, M. C., Treseder, K. K., Welp, L. P., Chapin, F. S., Harden, J. W., Goulden, M. L., Lyons, E., Neff, J. C., Schuur, E. A. G., & Zender, C. S. (2006). The impact of Boreal Forest Fire on Climate Warming. *Science*, 311, 1130-1132.

- Rubio, E., Caselles, & Badenas, C. (1997). Emissivity measurements of several soils and vegetation types in the 8-14  $\mu\text{m}$  wave band: Analysis of two field methods. *Remote Sensing of Environment*, 59, 490-521.
- Rubio, E., Caselles, V., Coll, C., Valor, E., & Sospedra, F. (2003). Thermal infrared emissivities of natural surfaces: Improvements on the experimental set-up and new measurements. *International Journal of Remote Sensing*, 20(24), 5379-5390.
- Sánchez, J. M., Caselles, V., Nicolòs, R., Valor, E., Coll, C., & Laurila, T. (2007). Evaluation of the B-method for determining actual evapotranspiration in a boreal forest from MODIS data. *International Journal of Remote Sensing*, 28 (5-6), 1231-1250.
- Sánchez, J. M., Kustas, W. P., Caselles, V., and Anderson, M. (2008). Modelling surface energy fluxes over maize using a two-source patch model and radiometric soil and canopy temperature observations. *Remote Sensing of Environment*, 112, 1130-1143.
- Sánchez, J. M., Caselles, V., Nicolòs, R., Coll, C., & Kustas, W. P. (2009). Estimating energy balance fluxes above a boreal forest from radiometric temperature observations. *Agricultural and Forest Meteorology*, 149, 1037-1049.
- Santanello, J. A., & Friedl, M. A. (2003). Diurnal covariation in soil heat flux and net radiation. *Journal of Applied Meteorology*, 42, 851-862.
- Scott, R. L., Shuttleworth, W. J., Goodrich, D. C., & Maddock III, T. (2000). The water use of two dominant vegetation communities in a semiarid riparian ecosystem. *Agricultural and Forest Meteorology*, 105, 241-256.
- Seguin, B. & Itier, B. (1983). Using midday surface temperature to estimate daily evaporation from satellite thermal IR data. *International Journal of Remote Sensing*, 4 (2), 371-383.
- Shuttleworth, W., & Wallace, J. (1985). Evaporation from sparse crops: an energy combination theory. *Quarterly Journal of the Royal Meteorological Society*, 111, 1143-1162.
- Su, H., McCabe, M. F., Wood, E. F., Su, Z., & Prueger, J. H. (2005). Modelling evapotranspiration during SMACEX02: Comparing two approaches for local and regional scale prediction. *Journal of Hydrometeorology*, 6 (6), 910-922.
- Valor, E. & Caselles, V. (1996). Mapping Land Surface Emissivity from NDVI: Application to European, African, and South American Areas. *Remote Sensing of Environment*, 57, 167-184.
- Valor, E. & Caselles, V. (2005): Validation of the vegetation cover method for land surface emissivity estimation. In: *Recent Research Developments in Thermal Remote Sensing*, Kerala (India), Research Signpost, pp. 1-20.



## **Evapotranspiration**

Edited by Prof. Leszek Labedzki

ISBN 978-953-307-251-7

Hard cover, 446 pages

**Publisher** InTech

**Published online** 16, March, 2011

**Published in print edition** March, 2011

Evapotranspiration is a very complex phenomenon, comprising different aspects and processes (hydrological, meteorological, physiological, soil, plant and others). Farmers, agriculture advisers, extension services, hydrologists, agrometeorologists, water management specialists and many others are facing the problem of evapotranspiration. This book is dedicated to further understanding of the evapotranspiration problems, presenting a broad body of experience, by reporting different views of the authors and the results of their studies. It covers aspects from understandings and concepts of evapotranspiration, through methodology of calculating and measuring, to applications in different fields, in which evapotranspiration is an important factor. The book will be of benefit to scientists, engineers and managers involved in problems related to meteorology, climatology, hydrology, geography, agronomy and agricultural water management. We hope they will find useful material in this collection of papers.

### **How to reference**

In order to correctly reference this scholarly work, feel free to copy and paste the following:

Juan M. Sánchez, Vicente Caselles and Eva Rubio (2011). Understanding the Effects of Fires on Surface Evapotranspiration Patterns Using Satellite Remote Sensing in Combination with an Energy Balance Model, Evapotranspiration, Prof. Leszek Labedzki (Ed.), ISBN: 978-953-307-251-7, InTech, Available from: <http://www.intechopen.com/books/evapotranspiration/understanding-the-effects-of-fires-on-surface-evapotranspiration-patterns-using-satellite-remote-sen>

**INTech**  
open science | open minds

#### **InTech Europe**

University Campus STeP Ri  
Slavka Krautzeka 83/A  
51000 Rijeka, Croatia  
Phone: +385 (51) 770 447  
Fax: +385 (51) 686 166  
[www.intechopen.com](http://www.intechopen.com)

#### **InTech China**

Unit 405, Office Block, Hotel Equatorial Shanghai  
No.65, Yan An Road (West), Shanghai, 200040, China  
中国上海市延安西路65号上海国际贵都大饭店办公楼405单元  
Phone: +86-21-62489820  
Fax: +86-21-62489821



© 2011 The Author(s). Licensee IntechOpen. This chapter is distributed under the terms of the [Creative Commons Attribution-NonCommercial-ShareAlike-3.0 License](https://creativecommons.org/licenses/by-nc-sa/3.0/), which permits use, distribution and reproduction for non-commercial purposes, provided the original is properly cited and derivative works building on this content are distributed under the same license.

IntechOpen

IntechOpen